Journal of Power Sources 196 (2011) 4067–4071

Contents lists available at ScienceDirect

Journal of Power Sources

journal homepage: www.elsevier.com/locate/jpowsour

Short communication

Inner pressure characterization of a sealed nickel-metal hydride cell

D.J. Cuscueta*, H.R. Salva, A.A. Ghilarducci

Centro Atómico Bariloche-Comisión Nacional de Energía Atómica (CAB-CNEA), Consejo Nacional de Investigaciones Científicas y Técnicas (CONICET), Instituto Balseiro-Universidad Nacional de Cuyo (IB-UNCu), Av. Bustillo 9500, 8400 San Carlos de Bariloche, Argentina

ARTICLE INFO

Article history:
Received 17 November 2010
Accepted 22 November 2010
Available online 26 November 2010

Keywords:
Ni-MH battery
Inner pressure
Electrochemical characterization
Fast charge

ABSTRACT

This paper studies the electrochemical behaviour of the pressure inside a sealed Ni-MH cell due to gases evolved under different charge/discharge currents and states of charge (SOC). The work is focused to determine the best procedure to get fast charge and long cycle life without detrimental effects on the battery and possible hazards affecting the safety of the user. The device was studied under a wide range of charge current (0.1–5 C), establishing that optimum conditions to minimize the inner pressure during uninterrupted use are obtained if either charge rates up to 0.5 C or higher rates not surpassing 90% of the nominal capacity are employed. Charge times corresponding to the range between 80% and 130% of the nominal capacity were also tested, analyzing the effect of overcharges on inner pressure, discharge capacity, efficiency and integrity of the cell. It was verified that charging the cell up to 130% at 2 C rate reaches an inner pressure 5 times higher than that obtained at 0.5 C. High rate discharge was also characterized at uninterrupted use of the cell, demonstrating the importance of the cut-off discharge criterion at high rates, to avoid the inner gases accumulation due to incomplete discharge of electrodes and overcharge in a following electrochemical cycle.

© 2010 Elsevier B.V. All rights reserved.

1. Introduction

The active development of electric vehicles (EVs) and hybrid electric vehicles (HEVs) has been accompanied by advances in new batteries that require high technology for energy storage [1]. The energy density requirements for HEV are relatively low; however, specific power and power density requirements are very high. In addition, the modality of fast charge and working in a wide range of temperature (0–60 °C) are requirements technically necessary for HEV application [2,3].

The nickel-metal hydride (Ni-MH) battery is very competitive to be used as power source for HEV because it has high specific energy, high-power capability, inherent safety, design flexibility and it is environmental friendly [4–10]. In commercial Ni-MH batteries, the relative amounts of electrochemically active materials employed in the fabrication of the positive and the negative electrodes are usually so determined that the charge–discharge capacity of the battery is "positive-electrode limiting" [10,11].

Due to the electrochemistry of Ni-MH batteries, fast charge is a technologic challenge because it may lead to a remarkable increase in pressure inside a sealed cell. Overcharging Ni-MH batteries also causes the internal gas pressure to increase. This pressure increase is due to hydrogen evolution at the surface of the negative electrode and oxygen evolution at the surface of the positive electrode [12], as shown in the following equations for negative and positive electrodes respectively:

$$4H_2O + 4e^- \rightarrow 2H_2\uparrow + 4OH^- \quad (1)$$

$$4OH^- \rightarrow 2H_2O + O_2\uparrow + 4e^- \quad (2)$$

Nevertheless, in positive-electrode limiting batteries, the negative electrode has a sufficient reserve charge and thus hydrogen evolution on the electrode may not be a major issue. In addition, the oxygen generated on the positive electrode at the end of the charging process and during overcharging [13] can move through the separator and be transformed to water on the surface of the negative electrode by the following recombination reaction:

$$4MH + O_2 \rightarrow 4M + 2H_2O \quad (3)$$

This reaction avoids the inner pressure build up. However, it may increase if the electrodes are seriously deteriorated and the recombination process (as suggested in Eq. (3)) does not work properly [11,14,15]. For this process, the oxygen generated at the positive electrode diffuses principally through the empty spaces in the separator toward the negative plate [16]. Since the oxygen diffusion in the electrolyte is slow and its solubility low, the hydrogen and oxygen recombination process is very closely related to the amount of electrolyte [2,17]. The overall diffusion coefficient of oxygen will vary according to factors such as the separator saturation level and

* Corresponding author at: Centro Atómico Bariloche-Comisión Nacional de Energía Atómica, Av. Bustillo 9500, 8400 San Carlos de Bariloche, Argentina.
Tel.: +54 2944 44 5155; fax: +54 2944 44 5299.
E-mail address: cuscueta@cab.cnea.gov.ar (D.J. Cuscueta).

0378-7753/$ – see front matter © 2010 Elsevier B.V. All rights reserved.
doi:10.1016/j.jpowsour.2010.11.131

tortuosity, showing optimal oxygen transport at electrolyte saturation level of the separator between 20% and 30% [16]. When the electrode assembly is over wetted, the recombination process is slow, an indication that the electrolyte is a barrier for the oxidation reaction [17]. However, if the electrolyte inside Ni-MH cells is excessively reduced, the internal resistance will rise and the charge efficiencies are lowered, leading to performance deterioration of Ni-MH cells. Hu et al. [2] showed that after opening a sealed Ni-MH cell, subjected to many cycles at elevated temperatures and long-term overcharges, and putting it into an electrolyte container, a significant reduction of the charge voltage and an increase of discharge voltage were observed, indicating that the electrolyte inside the Ni-MH cells had been at least partly consumed.

In the last few years, many efforts have been made on the research of the inner pressure of Ni-MH batteries [13,18,19]. Yang and Liaw [18,19] have characterized a Ni-MH module with a nominal capacity (C_n) of 85 Ah under certain fast charge conditions and found that internal pressure of the cell is the most critical parameter to be controlled for fast charge processes under safe operation. Shi et al. [14] confirmed the hydrogen gas evolution from an MH electrode during overcharges in a laboratory-made cylindrical 8 Ah Ni-MH battery, and proposed a temperature-dependent pressure model to investigate the kinetics of hydrogen evolution during fast charge. Cha et al. [3] studied the behaviour of a sealed Ni-MH system regarding its ability to consume gaseous products generated during the overcharge stage. They found that the internal pressure of sealed Ni-MH cells can be kept under control if the current rate is not too high, and if there is sufficient excess charging capacity in the negative electrode. Zhang et al. [11] found that the pulse charging technique is an effective approach to reduce the internal pressure of the battery and to extend the battery cycle life.

The aim of this work is to characterize the inner pressure produced by gas evolution in a laboratory-made sealed Ni-MH cell. For this purpose, electrochemical charge and discharge of the cell were monitored under different current rates and states of charge, looking for optimum conditions of use considering performance, efficiency and safety.

2. Experimental procedure

$LmNi_4Co_{0.31}Mn_{0.31}Al_{0.42}$ (Lm = lanthanum rich mischmetal, 84 wt% La, 8 wt% Ce, balance other elements) intermetallic alloy was used as the active material of the negative electrodes. It was obtained using an induction furnace, by melting the constitutive elements inside a boron nitride crucible, under an inert atmosphere (Ar). In order to ensure the alloy homogeneity, the sample was re-melted twice during the fabrication. For the negative electrode preparation, 100 mg of active alloy were freshly crushed and sieved between a 44 and 74 μm mesh; the resultant particles were then mixed with an equal amount of teflonized black carbon (Vulcan XC-72 + 33 wt% PTFE), as mechanical and conductive supports. This mixture was pressed to 300 MPa within a cylindrical matrix. The electrode obtained was a disk-shaped, of 11 mm diameter and 1 mm thickness. The capacity of the negative electrode, calculated from the specific alloy capacity previously determined (314 mAh g^{-1} [20]) and the alloy mass, was 31 mAh approximately.

The positive electrode used in measurements was provided by INIFTA (La Plata, Argentina). It is a commercial $Ni(OH)_2$ electrode for aerospace use, with a capacity of 20 mAh, since the specific capacity of the positive electrode is 143 mAh g^{-1} [21], and the mass of the sample was tailored to 140 mg. Thus, the capacity of the negative electrode was 55% in excess over the positive electrode, confirming a "positive-electrode limiting" cell working condition. The final dimensions of the parallelepiped electrode were 8 mm × 8 mm × 0.74 mm.

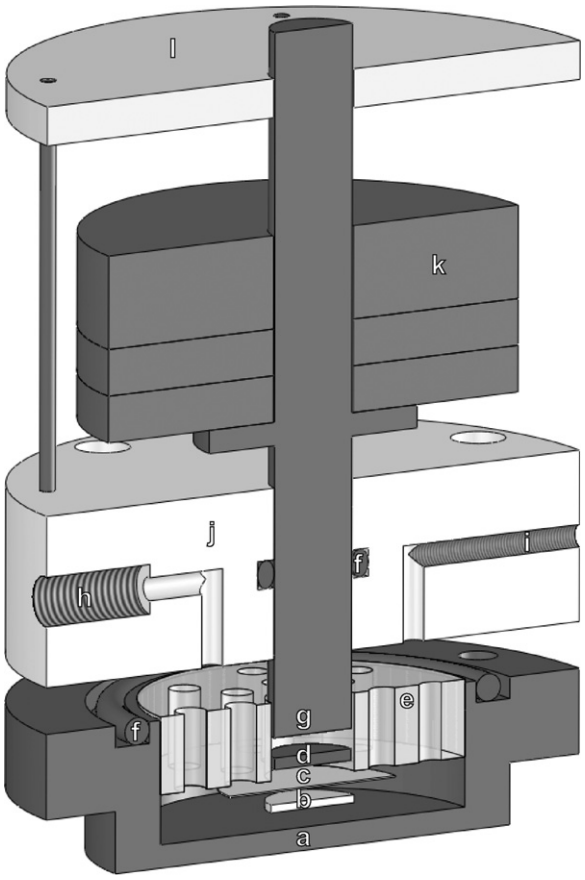

Fig. 1. Cross-section of cell used: (a) metallic base; (b) positive electrode; (c) separator; (d) negative electrode; (e) nylon piece for electrodes centring; (f) O-ring; (g) metallic piston; (h) duct for pressure transducer; (i) duct for purge; (j) nylon top; (k) masses for electrode compaction; (l) guide for piston.

The separator of the cell was a piece of woven roving glass-based material (RT200) provided by the Saint-Gobain Vetrotex Company, composed of E glass type, with a thickness of 150 μm and 204 g m^{-2} specific weight. The dimensions of the separators were adjusted to ensure insulation of the electrodes in the assembly.

Fig. 1 shows a cross-section of the cell used for electrochemical measurements [22]. It mainly consists of a metallic structure containing a moulding for the battery elements, i.e., electrodes, separator, electrolyte. The top of the system is composed by a cap and a metallic piston. Two O-rings seal the battery compartment and two ducts are placed for installing a pressure transducer and a screw for inner pressure purge. The electric path to the electrodes goes through the metallic base for the positive electrode and through the metallic piston for the negative electrode.

For electrochemical characterization, the electrodes and the separator assembled inside the cell were flooded with a concentrated solution of KOH 8 M as electrolyte, avoiding deterioration of cell performance by electrolyte consumption, but also working with a saturation level of the separator of nearly 100%. The electrochemical charge–discharge measurements on all experiments were performed at 23 °C, with an own laboratory developed galvanostat.

Table 1 shows some parameters of electrodes and electrolyte used in this work and compare them with those used by other researchers. It shows that the thickness of the positive electrode and separator of our setup configuration are similar to those used by other researchers in Ni-MH batteries. However, the negative electrode thickness is greater than the one used by other authors. This is due to the fabrication process because electrodes used in commercial developments are generally prepared by pressing solely

Table 1
Comparison between battery parameters used in our setup and by others.

Setup	Thickness (mm)			Saturation level (%)	
	Positive electrode	Negative electrode	Separator	Electrodes	Separator
Own	0.74	1	0.15	≈100	≈100
Others	0.60–1.00 [7,23–27]	0.15–0.50 [7,24,26,27]	0.12–0.21 [27,28]	70–80 [16]	≈70 [23]

the active alloy over a perforated foil or Ni foam, while in our case, we compact the active material with an equal quantity of teflonized carbon as support, leading to a thicker electrode. The fact that the saturation level of electrodes and separator is nearly 100% favours the ionic conductance but also hinders the diffusion for gases recombination.

For inner pressure measurements a Siemens transductor was used. The pressure range of the transductor is from vacuum to 600 kPa, and it is capable of working in corrosive environments.

The first 15 charge–discharge cycles were carried out to achieve the activation of the cell. The charge current was set to 10 mA for 2.4 h and the discharge current (I_d) was also fixed to 10 mA, while the cut-off discharge voltage was 600 mV.

After activation, the discharge capacity (C_d) and the inner pressure (P_i) were analyzed for charge current rates (I_c) from 0.1 C to 5 C. The discharge current rate was set to I_d = 0.5 C.

The P_i, C_d and energetic efficiency of the cell were subsequently studied for different charge times, varying these from 80% to 130% of the nominal discharge capacity. The study was performed for charge current rates between 0.5 C and 2 C, maintaining I_d at 0.5 C.

Finally, inner pressure and discharge capacity were analyzed as a function of the discharge current rate. For this purpose, the charge current was set to 1 C and discharge rates varied from 0.1 C to 5 C.

3. Results and discussion

Fig. 2 shows the cell potential and the inner pressure of gases inside the prototype during the first 15 electrochemical charge–discharge cycles. As the cell works in a positive-electrode limiting mode, the positive electrode gets fully charged first, so all excess of charge applied to the cell will produce the evolution of gaseous oxygen at the positive electrode [11]. Fig. 2 shows that inner pressure increases at the end of each charge period, i.e., during overcharge, reaching an equilibrium value of about 275 kPa along cycles. The gaseous oxygen evolved may recombine with the hydrogen of negative electrode to produce H_2O or OH^-, maintaining in the last case the electrolyte concentration. The rate of gases recombination is partially determined by the time required for O_2 to arrive at the negative electrode by crossing the separator, which

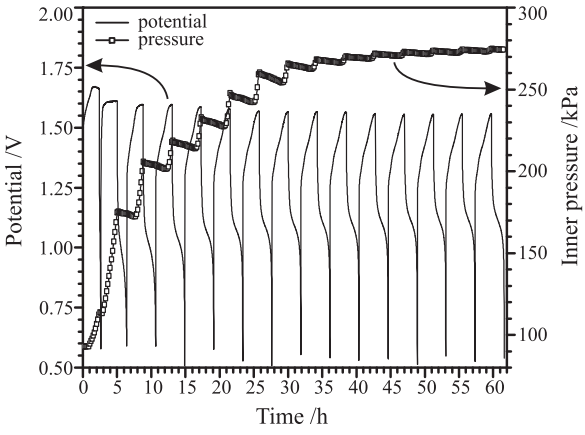

Fig. 2. Cell potential and inner pressure of gases during activation cycles.

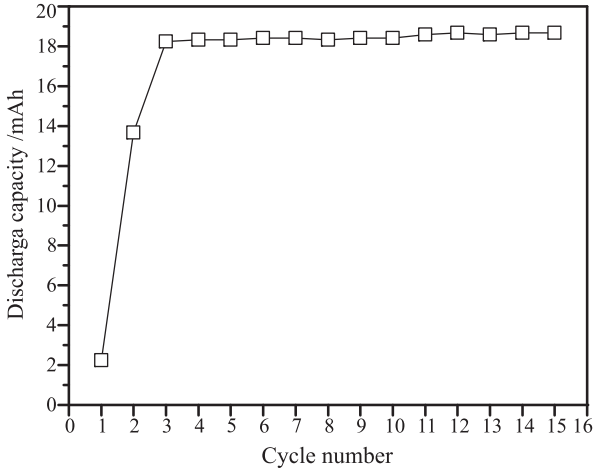

Fig. 3. Discharge capacity in the first 15 cycles.

is embedded in electrolyte with saturation level near 100%. The cell potential indicated by a continuous line in Fig. 2, reaches peaks of about 1.55 V during charge periods. The following discharges show plateaux between 1.1 V and 1.0 V, while the chemical reaction takes place at both electrodes.

Fig. 3 shows the discharge capacity obtained for each activation cycle. The battery is fully activated at the third cycle and reaches a maximum discharge capacity of 18.7 mAh, which is close to the intended limiting electrode value. The plateaux reached by cell inner pressure and discharge capacity ensure a stable working state of the cell to start pressure characterization. In order to analyze and compare its behaviour during different charge and discharge conditions, pressure curves are plotted subtracting the accumulated background, i.e., taking as base line the minimum pressure value obtained during charge.

Fig. 4 compares the P_i for I_c between 0.1 C and 5 C. For each current value, the charge time was adjusted to apply 120% of the nominal capacity, ensuring the complete charge of the cell. For a

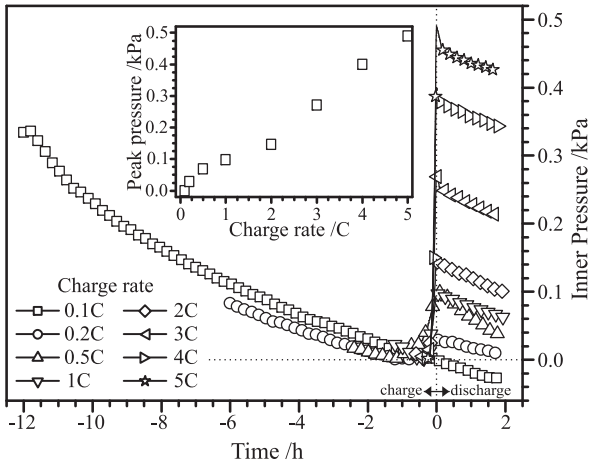

Fig. 4. Inner cell pressure for different charge rates.

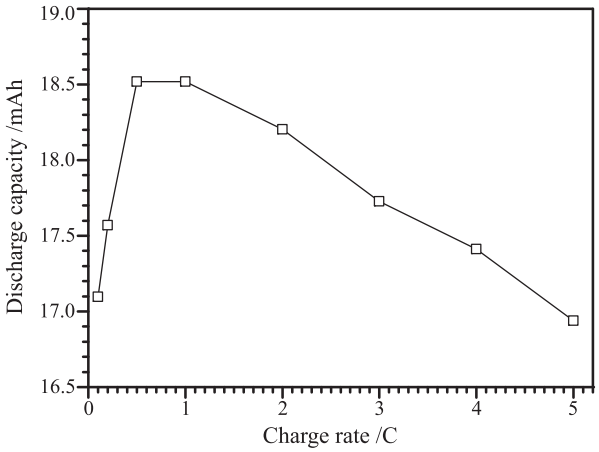

Fig. 5. Discharge capacity for different charge rates.

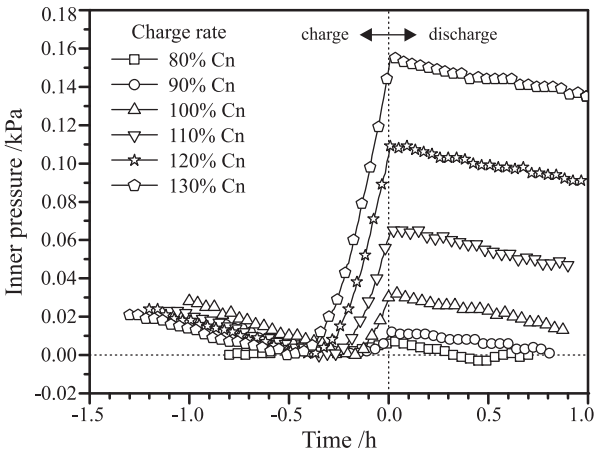

Fig. 6. Inner cell pressure for different charge times at C rate.

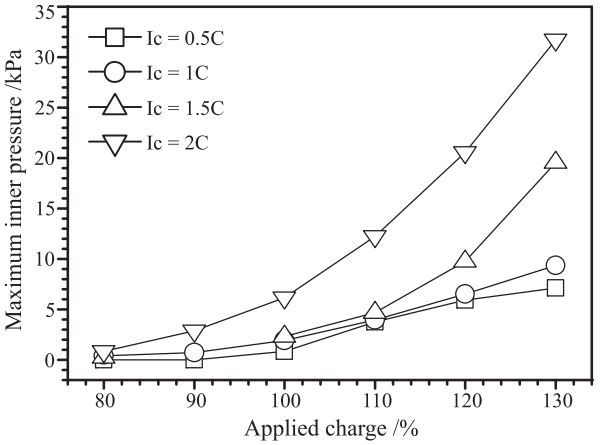

Fig. 7. Peak pressures for different times and rates of charge.

better graphical visualization, each end of charge time was considered as zero time, resulting negative time values for charges and positive for discharges.

A reduced graph inside Fig. 4 shows the peak pressure achieved for each charge rate. It is observed a linear relation between the charge rate and the maximum pressure inside the cell. Thus, higher rates allow for faster charges but may also lead to dangerous pressures, resulting in the opening of the safety valve of a commercial device and the exposure of the electrodes to further degradation. The construction of more robust commercial battery enclosures or the use of pressure control techniques may avoid this event. The recombination of gases may also be appreciated in Fig. 4, by the decrease of P_i during charge–discharge cycles. It may be seen that the remaining pressure inside the cell at the end of each cycle increases by as much as I_c does. Hence, in the continuous use of the cell, the remaining inner pressures may accumulate up to unsuitable levels. Since the discharge rate is usually set by the application requirement, it is recommended to control the charge rate in order to minimize this cumulative effect. The recombination rate, which is related to the saturation level of the separator by the electrolyte, is also an intrinsic variable for faster reducing the inner pressure of a cell, a subject that is beyond the scope of this work. Fig. 4 shows that for this particular system, the P_i at the end of each cycle is lower that the initial value only for charge rates of 0.1 C, 0.2 C and 0.5 C.

Fig. 5 shows the discharge capacity for different charge current rates. Values between 0.5 C and 1 C are optimal for largest discharge capacity. Comparing these results with those related to inner pressure, the charge rate of 0.5 C shows the best compromise; however, it is a low charge rate for applications requiring quick charge, like HEV.

In previous results, the complete charge of the cell was ensured by applying current during a period of time equivalent to 120% or more of C_n. What is studied here is the influence of the charge time on P_i for charge rates between 0.5 C and 2 C. Fig. 6 shows the results for charge times varying from 80% to 130% of C_n and for a charge rate of 1 C, showing how overcharges may increase P_i.

Fig. 7 summarizes the maximum values of P_i, for charge times varying between 80% and 130% of C_n, and for I_c between 0.5 C and 2 C. It is important to note that P_i is dependent not only on the charging time but also on I_c. From Fig. 7 one may conclude that P_i is more affected by the increase of I_c than by the charge time. This may be attributed to the hydrogen evolution in the MH electrode, due to the diffusion of adsorbed atomic hydrogen into the bulk of the alloy. This diffusion is not as fast as the accumulation of hydrogen on the electrode surface at the end of charge and during overcharge, producing build-up of hydrogen inside the cell. By comparing the evolution of P_i with the increase of charge time it may be seen that P_i grows exponentially, depending on the charge rate. Thus, the combination in a single graph of inner peak pressure for different currents and times of charge allows us to see that the increase of charge rate has a more harmful effect than overcharging the cell.

The energetic efficiency is determined by the relation between discharge capacity and applied charge. Fig. 8 shows the results of discharge capacity and efficiency for different times and rates of

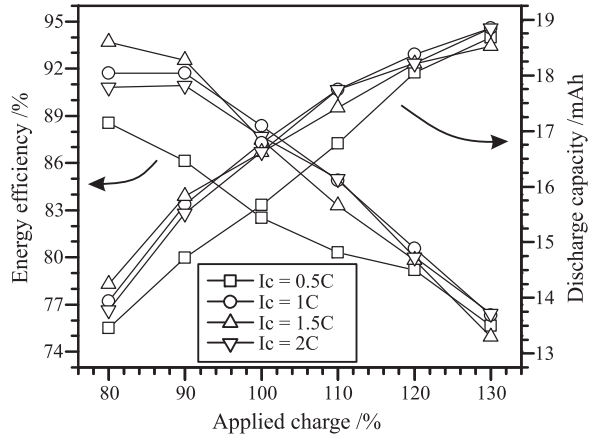

Fig. 8. Discharge capacity and efficiency for different times and rates of charge.

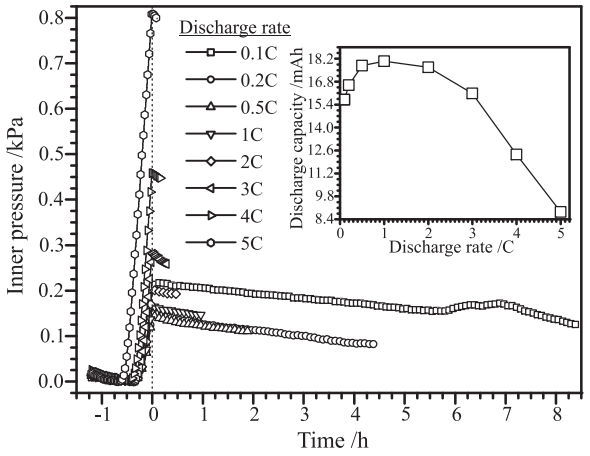

Fig. 9. Inner cell pressure and discharge capacity for different discharge rates.

charge. It shows how cell efficiency decreases while the discharge capacity increases with charging time. Therefore, the maximum cell efficiency is obtained for I_c greater than 0.5 C and for charge times between 80% and 90% of C_n. This indicates that overcharges are undesirable from the efficiency point of view.

Fig. 9 shows the results of inner pressure and discharge capacity for I_d between 0.1 C and 5 C. A first analysis of results could be interpreted as if P_i increases along with I_d. Nevertheless, this interpretation is not correct, due to the fact that the rates and times of charge were kept constant during the whole experiment. This behaviour is in fact produced because the higher the I_d, the higher the resistive losses occurring in contacts and electrolyte. This means that the effective potential of the cell is reduced proportionally to I_c. As the galvanostat was programmed for a fixed cut-off discharge potential of 600 mV, the reduction of the effective potential causes the incomplete discharge of the positive electrode. Thus, the cell is less discharged for higher I_d, producing an overcharge in the next cycle. As the discharge currents were scheduled to increase with each cycle, i.e., the first cycle with I_d = 0.1 C and last one with I_d = 5 C, the inner pressure increases with I_d. The detail in Fig. 9 shows the discharge capacity reached for each I_d studied, where maximum values occur for I_d between 0.5 C and 2 C.

4. Conclusions

The correct working of the cell was confirmed, becoming fully activated in the third electrochemical cycle and reaching a maximum discharge capacity of 18.7 mAh.

The study of inner pressure as a function of the charge rate confirms that for continuous use of the cell at I_d = 0.5 C and I_c up to 0.5 C, the mean value of the inner cell pressure does not increase. The maximum discharge capacity of 18.5 mAh was obtained for charging rates between 0.5 C and 1 C. For a 5 C charge rate capability, the discharge capacity was reduced by 8%.

The study of inner cell pressure for different times and rates of charge shows a compromise between the rates and times of charge and discharge to ensure that the recombination rate exceeds the gas evolution. Overcharges at rates higher than 1 C significantly increase the inner cell pressure. For example, when charging the cell to 130% of the nominal capacity at 2 C rate, the inner pressure reaches 32 kPa, 5 times higher than when overcharging at 0.5 C. However, efficient fast charge may be achieved by charging the cell up to 90% of nominal capacity.

Continuous cycling at high discharge rates may cause the incomplete discharge of the positive electrode due to ohmic losses, with inner pressure gradually increasing due to overcharging in subsequent cycles. For example, the continuous use of the cell at 5 C discharge rate increases the inner cell pressure by 0.8 kPa per cycle. This result shows the importance of the cut-off discharge criterion at high rates, to ensure the complete discharge of the battery.

Acknowledgements

The authors acknowledge to the Consejo Nacional de Investigaciones Científicas y Técnicas, Agencia Nacional de Promoción Científica y Tecnológica, Centro Atómico Bariloche and Instituto Balseiro for the financial support and to Prof. Linda Yael and Hernán A. Peretti for the English language revision.

References

[1] N. Sato, J. Power Sources 99 (2001) 70–77.
[2] W.K. Hu, M.M. Geng, X.P. Gao, T. Burchardt, Z.X. Gong, D. Noréus, N.K. Nakstad, J. Power Sources 159 (2006) 1478–1483.
[3] C. Cha, J. Yu, J. Zhang, Journal of Power Sources 129 (2004) 347–357.
[4] H. Ye, Y. Huang, J. Chen, H. Zhang, J. Power Sources 103 (2002) 293–299.
[5] P. Gifford, J. Adams, D. Corrigan, S. Venkatesan, J. Power Sources 80 (1999) 157–163.
[6] K. Wiesener, D. Ohms, G. Benczúr-Ürmössy, M. Berthold, F. Haschka, J. Power Sources 84 (1999) 248–258.
[7] T.-K. Ying, X.-P. Gao, W.-K. Hu, F. Wu, D. Noréus, Int. J. Hydrogen Energy 31 (2006) 525–530.
[8] S.R. Ovshinsky, M.A. Fetcenko, Appl Phys A 72 (2001) 239–244.
[9] U. Köhler, J. Kumpers, M. Ullrich, J. Power Sources 105 (2002) 139–144.
[10] M.L. Soria, J. Chacon, J.C. Hernandez, D. Moreno, A. Ojeda, J. Power Sources 96 (2001) 68–75.
[11] J. Zhang, J. Yu, C. Cha, H. Yang, J. Power Sources 136 (2004) 180–185.
[12] H.-K. Kim, D.-C. Yang, I.-S. Jang, C.-N. Park, C.-J. Park, J. Choi, Int. J. Hydrogen Energy 34 (2009) 9570–9575.
[13] A. Ayeb, P.H.L. Notten, Electrochim. Acta 53 (2008) 5836–5847.
[14] J. Shi, F. Wu, D. Hu, S. Chen, L. Mao, G. Wang, J. Power Sources 161 (2006) 692–701.
[15] D.-M. Kim, H. Lee, K. Cho, J.-Y. Lee, J. Alloys Compd. 282 (1999) 261–267.
[16] R. Nelson, J. Miner. Met. Mater. Soc. 53 (2001) 28–33.
[17] C. Wang, M. Marrero-Rivera, D.A. Serafini, J.H. Baricuatro, M.P. Soriaga, S. Srinivasan, Int. J. Hydrogen Energy 31 (2006) 603–611.
[18] X.-G. Yang, B.Y. Liaw, J. Power Sources 101 (2001) 158–166.
[19] B.Y. Liaw, X.-G. Yang, Solid State Ionics 152–153 (2002) 217–225.
[20] D.J. Cuscueta, A.A. Ghilarducci, H.R. Salva, R.H. Milocco, E.B. Castro, Physica B 404 (2009) 2848–2850.
[21] E.B. Castro, D.J. Cuscueta, R.H. Milocco, A.A. Ghilarducci, H.R. Salva, Int. J. Hydrogen Energy 35 (2010) 5991–5998.
[22] D.J. Cuscueta, A.A. Ghilarducci, H.R. Salva, Int. J. Hydrogen Energy (2010), doi:10.1016/j.ijhydene.2010.07.020.
[23] D. Linden, T.B. Reddy (Eds.), Handbook of Batteries, third ed., McGraw-Hill, New York, 2002, pp. 30.13.
[24] D.Y. Yan, Q. Cheng, T. Cui, J. Alloys Compd. 293–295 (1999) 809–813.
[25] W.K. Zhang, X.H. Xia, H. Huang, Y.P. Gan, J.B. Wu, J.P. Tu, J. Power Sources 184 (2008) 646–651.
[26] D. Yan, W. Cui, J. Alloys Compd. 293–295 (1999) 780–783.
[27] G.S. Nagarajan, J.W. Van Zee, J. Power Sources 70 (1998) 173–180.
[28] P. Kritzer, J. Power Sources 137 (2004) 317–321.